PCCP

PAPER

View Article Online
View Journal | View Issue

Cite this: *Phys. Chem. Chem. Phys.*, 2022, **24**, 5813

Mie scattering from optically levitated mixed sulfuric acid–silica core–shell aerosols: observation of core–shell morphology for atmospheric science

Megan R. McGrory,[ab] Rosalie H. Shepherd,[ab] Martin D. King, *[b] Nicholas Davidson,[c] Francis D. Pope, [c] I. Matthew Watson,[d] Roy G. Grainger,[e] Anthony C. Jones [fg] and Andrew D. Ward*[a]

Sulfuric acid is shown to form a core–shell particle on a micron-sized, optically-trapped spherical silica bead. The refractive indices of the silica and sulfuric acid, along with the shell thickness and bead radius were determined by reproducing Mie scattered optical white light as a function of wavelength in Mie spectroscopy. Micron-sized silica aerosols (silica beads were used as a proxy for atmospheric silica minerals) were levitated in a mist of sulfuric acid particles; continuous collection of Mie spectra throughout the collision of sulfuric acid aerosols with the optically trapped silica aerosol demonstrated that the resulting aerosol particle had a core–shell morphology. Contrastingly, the collision of aqueous sulfuric acid aerosols with optically trapped polystyrene aerosol resulted in a partially coated system. The light scattering from the optically levitated aerosols was successfully modelled to determine the diameter of the core aerosol (±0.003 μm), the shell thickness (±0.0003 μm) and the refractive index (±0.007). The experiment demonstrated that the presence of a thin film rapidly changed the light scattering of the original aerosol. When a 1.964 μm diameter silica aerosol was covered with a film of sulfuric acid 0.287 μm thick, the wavelength dependent Mie peak positions resembled sulfuric acid. Thus mineral aerosol advected into the stratosphere would likely be coated with sulfuric acid, with a core–shell morphology, and its light scattering properties would be effectively indistinguishable from a homogenous sulfuric acid aerosol if the film thickness was greater than a few 100 s of nm for UV-visible wavelengths.

Received 4th September 2021,
Accepted 19th November 2021

DOI: 10.1039/d1cp04068e

rsc.li/pccp

1 Introduction

Stratospheric aerosols have a large impact on the Earth's climate;[1–7] the scattering of incoming solar radiation[8] depends on the shape, composition and refractive index of the aerosol.[5,9,10] Quantification of the optical properties of stratospheric aerosol is needed to fully understand the influence of stratospheric aerosols upon the planet's radiative balance.[11]

Sulfuric acid aerosols are relatively abundant in the stratosphere:[12–14] the number density of sulfuric acid in the stratosphere has been determined from balloon-borne mass spectrometer experiments to be 10^4–10^5 molecules cm^{-3} below an altitude of 30 km and 10^6–10^7 molecules cm^{-3} between 30 to 35 km.[15,16] Anthropogenic emissions, biogenic processes and volcanic emissions act as the major sources of stratospheric sulfuric acid.[17–19] Owing to the abundance of sulfuric acid within the stratosphere, the condensation of sulfuric acid onto other stratospheric aerosol occurs readily:[20,21] Saunders *et al.*[22] estimated an encounter occurring purely from Brownian motion between a mineral dust particle with a radii of 0.0015 μm and a sulfuric acid aerosol with radii of 0.25 μm would take approximately 4 days. Deshler *et al.*[23] demonstrated that volcanic eruptions have influenced stratospheric aerosol size distributions for twenty of the last thirty years. Glass fragments make up a large proportion (60 to 80%) of mineralogy from volcanic eruptions[24] and tend to become coated in sulfuric acid, as shown by U2 flights in Mount St Helen's ash cloud.[24] The formation of a thin film of sulfuric acid on a stratospheric

[a] *Central Laser Facility, Research Complex, STFC Rutherford Appleton Laboratory, Oxford, OX11 0FA, UK. E-mail: andy.ward@stfc.ac.uk*
[b] *Department of Earth Sciences, Royal Holloway, University of London, Egham, Surrey, TW20 0EX, UK*
[c] *School of Geography, Earth & Environmental Sciences, University of Birmingham, Birmingham, B15 2TT, UK*
[d] *School of Earth Science, University of Bristol, Wills Memorial Building, Bristol, BS8 1RJ, UK*
[e] *National Centre for Earth Observation, Atmospheric, Oceanic and Planetary Physics, University of Oxford, Parks Road, Oxford OX1 3PU, UK*
[f] *Met Office, Fitzroy Road, Exeter, EX1 3PB, UK*
[g] *College of Engineering Maths and Physical Sciences, University of Exeter, Exeter, EX4 4PY, UK*

mineral aerosol would change the refractive index of the mineral aerosol and hence change the amount of incoming solar radiation that the aerosol scatters.[25,26] Stratospheric mineral aerosol coated in a thin film of stratospheric sulfuric acid could effectively have the optical properties of (a) the mineral aerosol, (b) the mineral aerosol slightly modified by thin film development or (c) sulfuric acid resulting from a core–shell aerosol resembling the sulfuric acid shell to a first approximation.

In the study presented, the light scattering from an optically trapped silica bead coated in a thin film of sulfuric acid has been measured. The study will (a) determine that aqueous sulfuric acid can wet and uniformly coat a mineral aerosol particle to form an aerosol with core–shell morphology and (b) record the back-scattered, visible Mie the scattered light to size the aerosol and determine the refractive index and shell thickness. Additionally, the Mie scattering as sulfuric acid collides with polystyrene aerosol was monitored: in the presented study it was observed that sulfuric acid did not wet polystyrene aerosols, thus demonstrating the lack of core–shell geometry. The polystyrene-sulfuric acid system provides an exemplar of a control experiment to demonstrate that a Mie spectrum for a non core–shell morphology is readily apparent in the Mie scattering. Comparison between the two systems that used either silica or polystyrene as the core aerosol provided additional evidence for the formation of core–shell aerosol when sulfuric acid collided with silica aerosol.

Atmospheric films on liquid or solid aerosols have been studied previously[25–42] and inorganic coatings on atmospheric aerosol have also been investigated.[26,27,43–45] For example, Rkiouak *et al.*[26] applied Raman spectroscopy to follow the development of sulfuric acid films on silica aerosol, whilst Tang *et al.*[44] studied the heterogeneous reaction of N_2O_5 on silica particles. Film development on atmospheric aerosols has previously been studied through application of optical trapping techniques.[26,27,38] For example, Jones *et al.*[25] determined the refractive index change as a film of oleic acid developed on a silica aerosol. Organic coatings of liquid core particles with a mixture of organic materials (from the oxidation of α-pinene) have also been studied.[46–50] Other studies have focused on the deliberate injection of particles into the stratosphere as a method of combating climate change.[10,21,51–53] It is reported that the injection of particles with a large refractive index may greatly increase the amount of solar radiation reflected back to space. Sulfates released into the stratosphere (and which later convert into sulfuric acid[54]) have been suggested as a material to purposefully implant into the stratosphere.[55] However, very little attention has been given to the microphysical interactions between the perturbing material and the ambient stratospheric aerosol layer. Owing to the composition and size of the acid aerosols,[51] sulfuric acid does not have the desirable characteristics of a highly reflective aerosol and therefore recent studies have begun to explore other, non-sulfate possibilities such as silica or titania.[27,51] Understanding how a thin film of sulfuric acid alters the scattering properties of the mineral aerosol is crucial to estimate how effective mineral aerosols are at scattering solar radiation.

2 Experimental

To investigate the light scattering from a sulfuric acid film of varying thickness upon a mineral aerosol, single mineral aerosols were optically levitated using vertically aligned, counter-propagating laser beams.[56–59] The counter-propagating laser beams provided a contact free method of levitating aerosols, allowing a replication of airborne processes with the correct aerosol morphology. Mie theory was applied to the backscattered spectrum to determine aerosol radius and refractive index using the relationship between wavelength and refractive index expressed in the Cauchy equation:[60]

$$n = A + \frac{B}{\lambda^2} + \frac{C}{\lambda^4} \quad (1)$$

where the unknown parameters can be determined as a function of wavelength. Within the Cauchy equation, n is the refractive index, λ is wavelength and A, B and C are the Cauchy coefficients. To study core–shell systems, it was important to study the core and shell material separately at the beginning of the study. The application of Mie theory allowed the refractive index of sulfuric acid aerosols and the refractive index and size of the core mineral aerosol to be determined prior to formation of a core–shell system. Afterwards, a film of sulfuric acid could be formed on the silica aerosol from a mist of sulfuric acid in air generated from a bulk aqueous sulfuric acid solution. The airborne aqueous sulfuric acid aerosols wetted and spread on the core mineral aerosol. Backscattered white light was recorded as a function of wavelength to produce a Mie spectrum. Mie spectra were continuously collected whilst sulfuric acid aerosols collided with the silica aerosol; the experimental Mie spectra were then simulated allowing the refractive index, radius and film thickness of the core–shell system to be characterised. For the purpose of the study, silica was used as a proxy-mineral aerosol.

2.1 Sulfuric acid and silica aerosol

VWR Chemicals supplied aqueous sulfuric acid as a 50% w/w solution. Dilutions were made by weight using water with conductivity below 18 MΩ cm^{-1}. Spherical silica beads were sourced from Bangs Laboratories Inc., product number SS04N, lot number 7920. The beads are reported as non-porous with a reported density of 2 g cm^{-3} and a radius of approximately 1.035 μm. To determine the refractive index and radius of a trapped aerosol Mie spectroscopy requires the shape of the aerosol to be accurately known, and thus use of mineral aerosol samples extracted from the atmosphere was not possible. Additionally, Bangs Laboratories Inc. supplied polystyrene beads: product number PS04N, lot number 12 487. The polystyrene beads had a density of 1.04–1.15 g cm^{-3} and a radius of approximately 1.04 μm.

2.2 Aerosol generation

An ultrasonic nebuliser (aerosonic travel ultrasonic nebuliser) delivered sulfuric acid aerosols to the sample cell. The radius of the trapped aqueous sulfuric acid aerosol varied from 0.1 μm to

over 5 μm. Aerosols in the range 1.4 to 2.0 μm were used for Mie scattering studies. An atomiser (Topas, ATM 220) with diffusion dryer (Topas, DDU 570/L) was used to deliver silica and polystyrene to the sample cell from aqueous suspensions. Prior to atomisation, the silica or polystyrene beads were dispersed in water at a concentration of 2% w/w.

2.3 Optical trapping

A 1064 nm, continuous wave Nd:YAG laser beam (Ventus, Laser Quantum) was split into two paths. The beams were delivered, *via* beam expansion optics, to two opposing microscope objective lenses (Mitutoyo NIR × 50, NA 0.42) that focused the two beams to form an optical trap.[62] A piezo-stage (Physik-Instrumente) was used to control the x, y and z positions on the upper laser beam pathway allowing accurate alignment of the focused beams. The power of the laser beam at the point of focus was set to 10 mW for the upward propagating beam and 15 mW for the downwards propagating beam. A simplified schematic of the optical trapping equipment is depicted in Jones *et al.*[57] Optical trapping techniques have recently been reviewed.[63] A custom-made aluminium sample cell was used as a chamber to trap the aerosols. The cell had two-quarter inch fittings to allow entry of the aerosols and to provide an exhaust path. Windows at the top and bottom allowed the laser beam to enter the cell. Brightfield illumination was configured along the same axis using the lower microscope objective for imaging, with an optical filter to attenuate the laser wavelength. The radius of the trapped aerosol was estimated from images with a resolution of 0.5 μm to provide a coarse starting value for aerosol size when modelling the Mie light scattering with wavelength. Brightfield sources were isolated whilst a spectrum was acquired. Brightfield microscopy allowed imaging of aerosols and the surface. By raising the cover slip the trapped aerosol particle could be placed in a clean location to permit inspection. The deposited aerosol was imaged to validate that a silica bead, surrounded by liquid, formed the final aerosol.

2.4 Acquisitions and modelling of Mie spectra

A white-light LED was focussed on the trapped aerosol and the elastic, backscattered light collected using the microscope objective; the light was then dispersed by a spectrometer onto a charge-coupled device detector (Princeton Instrument Spec 10:400 BR), which recorded light intensity as a function of wavelength. Typically a 600 line mm^{-1} grating dispersed the collected light across a wavelength range of 520 to 600 nm with a resolution of 0.06 nm per pixel as shown in Fig. 1. Henceforth, in the study presented, the spectrum of the intensity of backscattered light *versus* wavelength will be called a Mie spectrum. An argon pen-ray lamp was used for the wavelength calibration of the spectrometer. To determine the refractive index and radius of the trapped aerosol, the experimental Mie spectrum was compared to a calculated Mie spectrum produced through application of Mie theory based on Bohren and Huffman;[64] the radius and refractive index was varied until a global minimum was determined with the least squares fitting residual between experimental and theoretical peak positions.[57,65] Additionally,

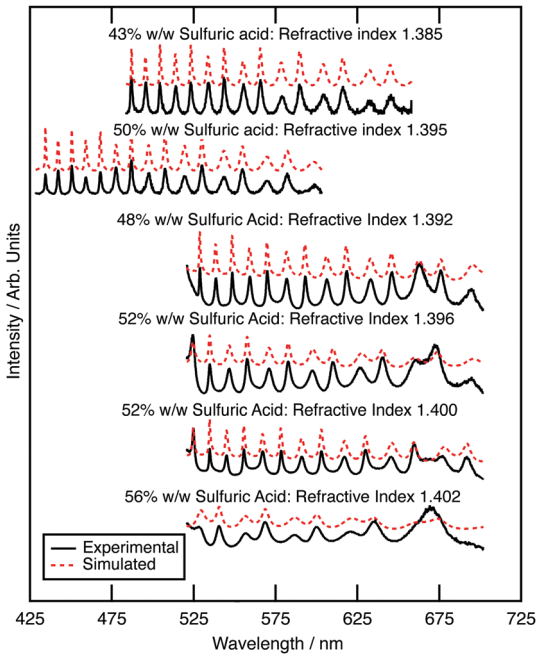

Fig. 1 Measured and simulated Mie spectra for optically trapped sulfuric acid aerosols, each of the six spectra represent a sulfuric acid aerosol that originates from a different concentration bulk aqueous sulfuric acid solution. Simulated Mie spectra for each experimental Mie spectra are additionally shown. The displayed spectra are offset to provide a clear depiction of the spectra. The wavelengths ranges were different in different experiments to widen the wavelength range of the study slightly.

core–shell Mie theory[66,67] was applied to calculate the Mie spectra of the core–shell silica–sulfuric acid aerosol; the calculated spectra simulated a series of sulfuric acid films of known thickness on a silica aerosol of known radius and refractive index. The calculated Mie spectra were then compared to experimentally collected core–shell Mie spectra to determine the thickness of the acid film. Further advances in the efficient modelling of core–shell Mie modelling can be found elsewhere.[68,69]

3 Results and discussion

3.1 Sulfuric acid

The optical properties of aqueous sulfuric acid has been characterised for a range of sulfuric acid concentrations: Remsburg *et al.*[70] studied aqueous sulfuric acid in the concentration range 75 to 90% w/w, whilst Palmer and Williams[71] studied the concentration range 25 to 95.6% w/w. In more recent years, studies have begun to determine the optical properties of sulfuric acid in stratospheric-like conditions. Tisdale *et al.*,[72] Niedziela *et al.*,[73] Steele *et al.*,[74] Wagner *et al.*,[75] and Lund-Myhre[76] studied the effect of temperature upon the optical properties of sulfuric acid droplets, whilst Wagner *et al.*[77] investigated the change in refractive index as a sulfuric acid system was supercooled. All have shown that the refractive index of sulfuric acid is dependent on temperature at Infrared wavelengths and Krieger *et al.*[61] have shown that the refractive

index of sulfuric acid at visible wavelengths is also dependent on temperature, with a determined refractive index of 1.40 at 20 °C, and 1.42 at −60 °C (at wavelength 533.5 nm and concentration 52.5 wt%). The refractive index of the sulfuric acid in this study at room temperature will therefore differ from that at the coldest stratospheric temperatures.

In the study presented here, precursory experiments to determine the optical properties, and hence concentration, of optically trapped aqueous sulfuric acid aerosols were paramount for calculation of core–shell silica–sulfuric acid systems; the refractive index of optically trapped sulfuric acid was required to create accurate simulations of core–shell silica–sulfuric acid aerosol. Bulk aqueous solutions with the concentrations of 5, 10, 15 or 20% w/w were prepared and nebulised separately to deliver aerosols to the optical trap.[78] The Mie spectrum for each aerosol was obtained: Fig. 2 depicts the experimental and calculated Mie spectra for the aqueous sulfuric acid aerosols for each initial concentration. The refractive index and radius of the optically trapped aerosols are summarised in Table 1. The refractive index can be determined with a precision of 0.007, whilst the radius of the aerosol was determined to ±0.003 μm.

Fig. 2 compares the refractive index dispersion for the optically trapped sulfuric acid aerosols to literature refractive index dispersions for bulk aqueous sulfuric acid solutions of known mass ratio.[79] The refractive index for experimental sulfuric acid aerosols lie at a refractive index of approximately 1.395 ± 0.007 at 589 nm, which corresponds to a mass ratio of 50 ± 4 w/w%. The mass ratio of sulfuric acid to water of the optically trapped aerosols has increased upon trapping; water has evaporated. The relationship between sulfuric acid concentration and the surrounding environment was demonstrated by Mund and Zellner,[80] in particular showing a dependence on the local relative humidity and temperature of the surrounding environment. The relative humidity of the laboratory was measured between 30 and 35 percent during these experiments, which is commensurate with an equilibrium of 50 to 53 w/w% sulfuric acid.[81] The sulfuric acid to water ratio is controlled by local relative humidity, and this is refined by the microenvironment of the aerosol. Separate testing on the aerosol sample cell, to explore the behaviour of the relative humidity within the cell, found that extreme prolonged nebulisation floods the chamber with an aqueous sulfuric acid mist, coats the windows of the cell, and will result in a local humidity environment that controls the concentration of sulfuric acid within the droplet. Such experiments were undesirable and easily avoided. The experiment described here utilised a 5 second nebulisation, which was sufficient to capture or collide a single droplet. On separate tests this gave a transient RH increase of a few % (~6%) which returns back to room RH in a few minutes. For all experiments hereafter, it is assumed that nebulised sulfuric acid aerosols will equilibrate with the surrounding environment to reach a concentration of 50% w/w with a refractive index of 1.395 ± 0.007 at 589 nm; the assumed refractive index will be used in calculations of core–shell silica–sulfuric acid aerosol.

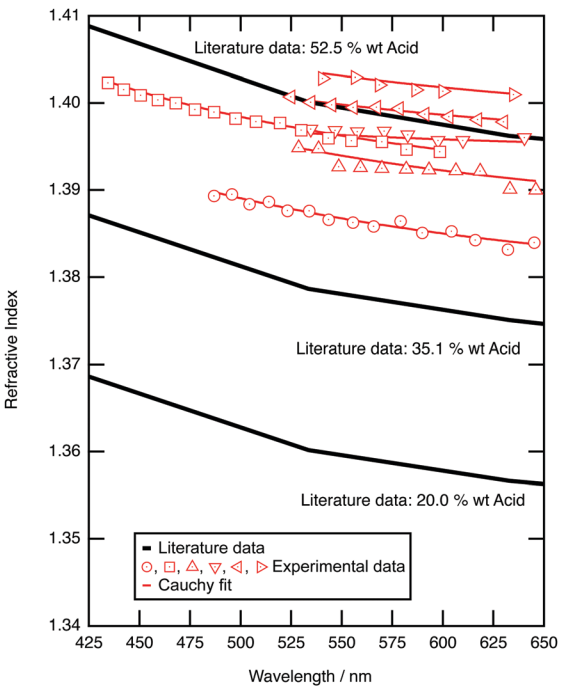

Fig. 2 Experimental (red diamond) refractive index of trapped sulfuric acid aerosols as a function of wavelength are compared to literature values for aqueous sulfuric acid solutions that have different mass ratios of sulfuric acid to water at a temperature of 21 °C.[61]

3.2 Silica aerosol

Simulation of Mie spectra for core–shell aerosols requires the size and refractive index of the core aerosol to be measured first. The silica Mie spectrum depicted in Fig. 3 is typical of mineral aerosol.

Eighteen separate silica beads were individually optically trapped and gave an average and standard deviation radius of 0.958 ± 0.005 μm, whilst the refractive index was measured as 1.383 ± 0.018 at 589 nm. The variation in values of refractive index with wavelength were calculated to be 1.374 ± 0.018, 2763 ± 483 nm^2 and 1 × 10^8 nm^4 for A, B and C respectively as defined in eqn (1). The measured values of refractive index for silica is notably lower than published values, for example 1.458 at 589 nm was determined by Malitson *et al.*[79] Variation in refractive index for different silica samples could be attributed to the mass density of silica.[25] The density determined by the manufacturers and our own densitometer measurements is also lower than bulk silica. Previously low refractive index values of silica beads has been attributed to particle porosity as demonstrated by Tisdale *et al.*[82] who measured the refractive index for silica beads to range from 1.38 to 1.42; increased porosity would reduce the density of the bead.

3.3 Sulfuric acid film growth on silica aerosol

Mie spectra of the optically trapped aerosol were obtained throughout the collision of sulfuric acid with silica aerosol. Fig. 3 depicts the Mie light scattering spectra during growth of a film of sulfuric acid upon the silica. The film thickness of the

Table 1 The mass ratio of sulfuric acid aerosols increased upon trapping, as determined by Mie theory. *A*, *B* and *C* are the Cauchy coefficients from eqn (1)

Bulk sulfuric acid	Sulfuric acid droplet					
Concentration/% w/w	Radius/μm	Concentration/% w/w	Refractive index (589 nm)	*A*	*B*/nm^2	*C*/nm^4
5	1.349 ± 0.006	56	1.402 ± 0.007	1.395	2425	1.0×10^7
10	1.459 ± 0.006	50	1.395 ± 0.007	1.386	3105	7.9×10^5
10	1.709 ± 0.006	43	1.385 ± 0.007	1.376	3237	7.4×10^6
10	1.733 ± 0.006	52	1.400 ± 0.007	1.393	2210	3.0×10^6
15	1.605 ± 0.006	52	1.396 ± 0.007	1.394	425	8.5×10^7
20	1.785 ± 0.006	48	1.392 ± 0.007	1.384	2750	8.0×10^7

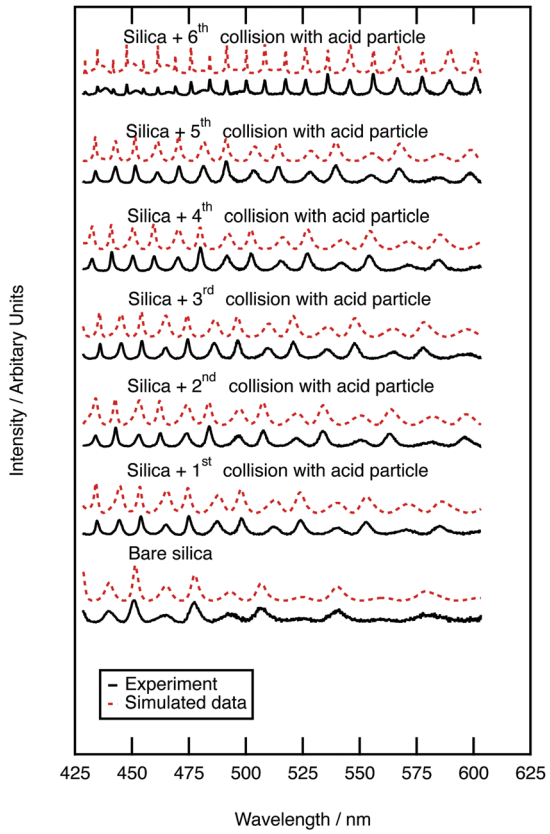

Fig. 3 Mie spectra showing how the Mie scattering of silica aerosol alters upon growth of a film of sulfuric acid. Core–shell Mie theory was applied to determine thickness of the developing shell, the Mie theory simulations are depicted with red, dashed lines. Six collisions are depicted: the first collision formed a film of sulfuric acid on the silica of thickness 0.262 μm, whilst the subsequent collisions thickened the film further to a total film thicknesses of 0.287, 0.321, 0.337, 0.369, 0.824 μm.

sulfuric acid film was calculated by assuming a constant silica core surrounded by a shell of increasing thickness with the refractive index of a 50% w/w aqueous sulfuric acid solution. After the first collision, the thickness of the acid film was 0.262 ± 0.0003 μm, requiring a sulfuric acid aerosol with a volume of 4.097 μm^3 to collide with the silica aerosol. After the second collision the film was 0.287 ± 0.0003 μm thick; to develop the film a second sulfuric acid aerosol with a volume of 0.496 μm^3 collided with the silica aerosol. To determine whether the film of sulfuric acid alters the light scattering properties of the core silica aerosol, the Mie scattering properties of the core–shell aerosol were compared with those of pure sulfuric acid. The product of the first collision had a radius of 1.244 ± 0.0003 μm, and has a similar Mie spectrum to a sulfuric acid aerosol with a larger radius of 1.246 μm. The product aerosol particles from the second and all of the subsequent collisions had Mie spectra similar to that of a pure homogenous aerosol particle with the same radius as a core–shell aerosol within error. Therefore, we infer that when a micron-sized sulfuric acid aerosol collides with an optically trapped silica aerosol the resultant core–shell aerosol will begin to resemble a sulfuric acid aerosol of the same diameter as the shell becomes thicker.

3.4 Sulfuric acid film growth on polystyrene aerosol

As further evidence for demonstrating the sensitivity of the technique to core–shell aerosol formation, a system unlikely to form a core–shell system was chosen. Hydrophobic polystyrene aerosols were trapped and the collision of aqueous sulfuric acid with the polystyrene followed with Mie spectroscopy. Fig. 4a depicts calculated core–shell Mie spectra as a film of sulfuric acid develops on a polystyrene aerosol; the simulation shows an increase in the number of resonances as the film thickens. Contrastingly, the experimental results depicted in Fig. 4b demonstrate a loss of resonances as the sulfuric acid collided with the polystyrene aerosol. The contrast in Mie spectra shown in Fig. 4a and b indicate that sulfuric acid and polystyrene do not form a core–shell geometry. Owing to the contrast in hydrophobic and hydrophilic nature of polystyrene and aqueous sulfuric acid, the condensation product may represent a partially engulfed system.[46,83] Phase separation between contrasting liquids in aerosols has been extensively studied.[84–87] In particular, Reid *et al.*[83] investigated the morphology of mixed phase systems through application of optical trapping techniques; concentrating on compounds containing hydrophobic and hydrophilic domains demonstrated that systems containing partitioning constituents do not always form core–shell morphology.

3.5 Stratospheric implications

Owing to the relative abundance of sulfuric acid aerosols residing in the stratospheric aerosol layer,[12–14] the consequences of the collision of sulfuric acid aerosols with solid aerosols is highly relevant to understanding the optical scattering efficiency of the stratosphere. The difference in optical properties of a coated aerosol in comparison to an uncoated sphere has

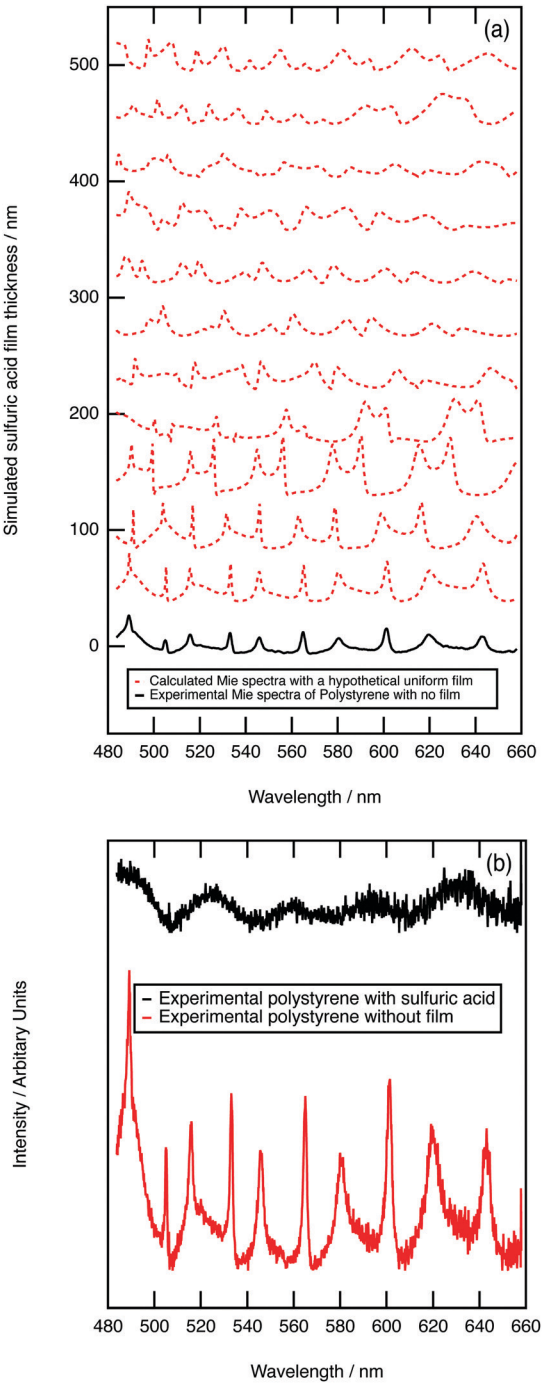

Fig. 4 Graphs depicting (a) the Mie-theory simulated spectra for sulfuric acid film development on the experimental obtained Mie spectrum for pure polystyrene and (b) the experimentally obtained Mie spectra for the growth of a film of sulfuric acid on polystyrene.

drawn significant attention in recent years:[25,88–92] in particular Kahnert *et al.*[90] has modelled the encapsulation of aggregates by a sulfate film whilst Soewono and Rogak[89] and Wu *et al.*[91] have explored the effect of a sulfate film on a soot particle.

The core–shell geometry formed by aqueous sulfuric acid on silica in this work relies on the aqueous sulfuric acid being liquid at typical stratospheric temperatures (−56.5 °C to −2.5 °C for a standard atmosphere[81]). Homogenous freezing processes in the atmosphere are non-trivial *e.g.* ref. 93–95 and important for cloud formation processes *e.g.* ref. 96. There have been many determinations of the homogenous freezing of aqueous sulfuric acid,[73,96–110] which have been collated as a function of water activity.[96] Using figure D1 from Scheider *et al.*,[96] which is adapted from Koop,[94] demonstrates that aqueous solutions of sulfuric acid around 50%v/v have freezing temperature below −70 °C and thus for the work presented here freezing of the aqueous sulfuric acid affecting the core–shell morphology at stratospheric temperatures need not be considered.

As demonstrated in the study presented, sulfuric acid collides with a silica aerosol, wets and spreads over the surface of the silica aerosol to form a symmetrical core–shell aerosol. Laboratory experiments, at room temperature and pressure, demonstrated that the light scattering properties of the core–shell aerosol system moved rapidly away from the mineral aerosol, and began to represent the Mie spectra of a pure aqueous sulfuric acid aerosol. Assuming similar core–shell behaviour at the lower temperatures and pressures of the stratosphere the light scattering efficiency, Q_{scatter} of a typical silica spherical aerosol particle was calculated using the Mie Code described in the methodology as function of sulfuric acid film thickness and compared to a similar-sized homogenous spherical sulfuric acid particle and a similar sized homogenous spherical silica aerosol particle. The calculation was performed at UV, visible, and near-IR wavelengths of light to demonstrate a similar effect at these wavelengths of light. These wavelengths were chosen as refractive index data for sulfuric acid have been reported as a function of temperature (~273 K) and composition (~52% w/w sulfuric acid).[61] Values for the silica core aerosol were taken from Malitson[79] for the same wavelengths. For the core–shell particle the initial silica core radius was 0.40 μm as the median core radius, r_{m},[23,24] for a log-normally distributed silica particle size distribution with a geometric standard deviation, σ, of 1.5. Number densities, N, of atmospheric aerosol are typically log-normally distributed around a median radius, r_{m} with a geometrical standard deviation, σ, formulated in eqn (2), where, N_0 is the total number of particles in the distribution.[111]

$$\frac{\mathrm{d}N}{\mathrm{d}\ln(r)} = \frac{N_0}{\sqrt{2\pi}} \frac{1}{\ln(\sigma)} \mathrm{e}^{-\frac{\ln(r)-\ln(r_{\text{m}})}{2\ln^2(\sigma)}} \quad (2)$$

The efficiency of light scattering, Q_{scatter} at different sulfuric acid shell thicknesses (with a fixed core radius of 0.4 μm) are calculated across the log-normal distribution and weighted by the number density calculated using eqn (2). The shell thickness was increased in 0.03 μm increments until the total radius of the core–shell system had reached 2.40 μm. The results are compared to the scattering efficiency, Q_{scatter} of a pure homogenous sulfuric acid aerosol particle and a pure homogenous silica aerosol particle in Fig. 5. Fig. 5 demonstrates that the structure of the scattering efficiency of the core–shell aerosol particle begin to represent the shell sulfuric acid quickly; similar results were determined with the laboratory results.

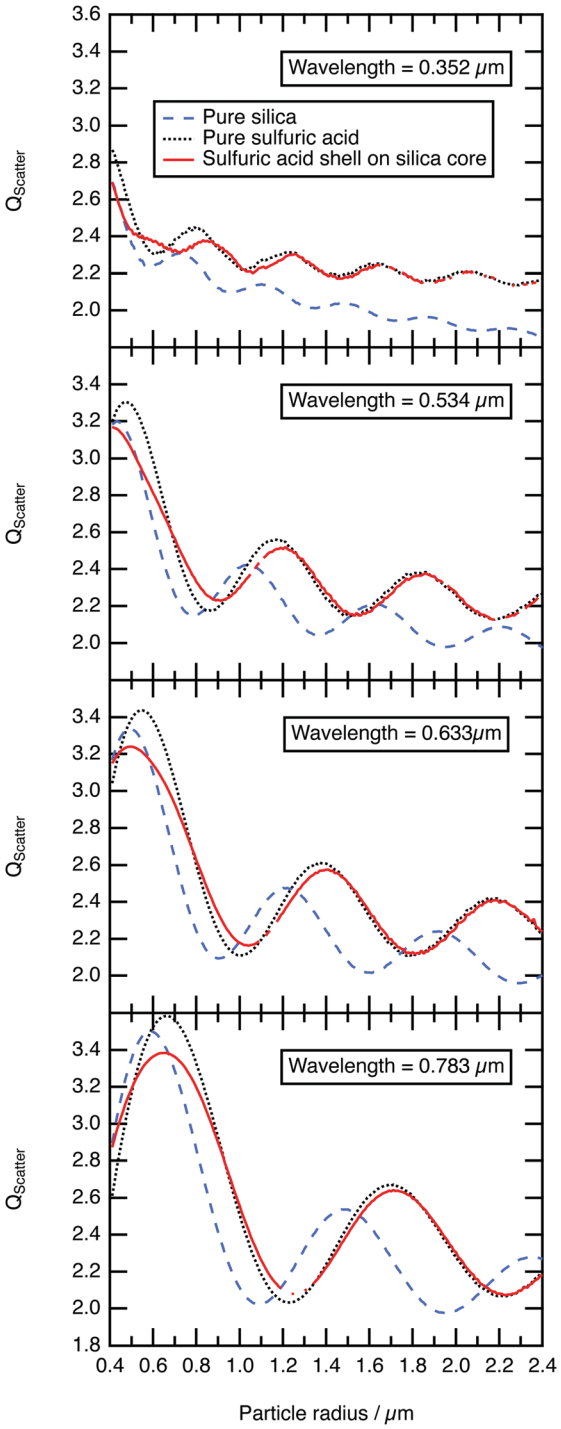

Fig. 5 $Q_{scatter}$ calculated for a core–shell spherical particle with a 0.4 μm radius silica core and an increasing uniform sulfuric acid shell, compared with homogenous spherical particles of silica, and sulfuric acid with increasing radius. Each value of $Q_{scatter}$ is weighted for a log-normal distribution about a median radius corresponding to the particle radius of the ordinate, with a geometric standard deviation of 1.5. Initially the core–shell particle has a similar value of $Q_{scatter}$ to the silica particle and then within a 0.4–0.75 μm film thickness of sulfuric acid is indistinguishable from pure sulfuric acid.

As explained in Section 3.3, Mie spectra of optically trapped core–shell aerosol represented the Mie spectra of pure aqueous sulfuric acid when the film of the aqueous sulfuric acid becomes thicker. Additionally, Fig. 5 depicts the structure and intensity of the scattering efficiency for the core–shell system and sulfuric acid aligning once a film 0.4–0.75 μm thick had developed. Consequently, the formation and resultant optical properties of core–shell aerosols ought to be carefully considered in future modelling of stratospheric aerosols.

4 Conclusions

The study presented here demonstrates that sulfuric acid successfully forms a core–shell geometry aerosol upon collision with silica. Through application of optical trapping techniques alongside Mie spectroscopy, it was observed that when a sulfuric acid aerosol collides with a silica aerosol, the system would begin to resemble a sulfuric acid aerosol of similar diameter to the combined aerosol. Secondly, the study experimentally demonstrates that mineral aerosol emitted to the stratosphere will soon adopt the light scattering patterns associated with a pure sulfuric acid aerosol. The implication of the study to stratospheric science is that hydrophilic stratospheric mineral aerosol will rapidly resemble the optical properties of sulfuric acid through natural collision processes and the formation of core–shell morphology.

Conflicts of interest

There are no conflicts to declare.

Acknowledgements

The authors are grateful for STFC for allowing access to the optical trapping laboratory at the Central Laser Facility, Rutherford Appleton Laboratories under the access grant 14230020. Rosalie H. Shepherd would like to thank STFC for funding the student grant ST\L504279\1. Megan McGrory would like to thank NERC for funding of grant NE\R012148\1. The work presented here has been supported by NERC grant NE/T00732X/1 for ADW and MDK. IMW was funded by EPSRC/NERC/STFC under EP/l01473X/1.RGG was funded as part of NERC's support of the National Centre for Earth Observation grant NE/R016518/1. ACJ was supported by a Met Office/NERC CASE (ref. 580009183) PhD studentship.

Notes and references

1 S. M. Andersson, B. G. Martinsson, J.-P. Vernier, J. Friberg, C. A. M. Brenninkmeijer, M. Hermann, P. F. J. van Velthoven and A. Zahn, *Nat. Commun.*, 2015, **6**, 7692.
2 R. Auchmann, F. Arfeuille, M. Wegmann, J. Franke, M. Barriendos, M. Prohom, A. Sanchez-Lorenzo, J. Bhend, M. Wild, D. Folini, P. Štěpánek and S. Brönnimann, *J. Geophys. Res.: Atmos.*, 2013, **118**, 9064–9077.
3 D. Baumgardner, G. Kok and G. Raga, *Geophys. Res. Lett.*, 2004, **31**, L06117.

4 C. Brühl, J. Lelieveld, H. Tost, M. Höpfner and N. Glatthor, *J. Geophys. Res.: Atmos.*, 2015, **120**, 2103–2118.
5 A. Lacis, J. Hansen and M. Sato, *Geophys. Res. Lett.*, 1992, **19**, 1607–1610.
6 G. Myhre, T. F. Berglen, C. E. Myhre and I. S. Isaksen, *Tellus B*, 2004, **56**, 294–299.
7 G. Pitari, G. Di Genova, E. Mancini, D. Visioni, I. Gandolfi and I. Cionni, *Atmosphere*, 2016, **7**, 75.
8 O. B. Toon and J. B. Pollack, *Am. Sci.*, 1980, **68**, 268–278.
9 A. J. Durant, S. P. Harrison, I. M. Watson and Y. Balkanski, *Prog. Phys. Geograph.: Earth Environ.*, 2009, **33**, 80–102.
10 A. C. Jones, J. M. Haywood and A. Jones, *Atmos. Chem. Phys.*, 2016, **16**, 2843–2862.
11 K. D. Beyer, A. R. Ravishankara and E. R. Lovejoy, *J. Geophys. Res.: Atmos.*, 1996, **101**, 14519–14524.
12 G. K. Yue, L. R. Poole, P.-H. Wang and E. W. Chiou, *J. Geophys. Res.: Atmos.*, 1994, **99**, 3727–3738.
13 D. M. Murphy, K. D. Froyd, J. P. Schwarz and J. C. Wilson, *Q. J. R. Meteorol. Soc.*, 2014, **140**, 1269–1278.
14 S. Kremser, L. W. Thomason, M. von Hobe, M. Hermann, T. Deshler, C. Timmreck, M. Toohey, A. Stenke, J. P. Schwarz, R. Weigel, S. Fueglistaler, F. J. Prata, J.-P. Vernier, H. Schlager, J. E. Barnes, J.-C. Antuña-Marrero, D. Fairlie, M. Palm, E. Mahieu, J. Notholt, M. Rex, C. Bingen, F. Vanhellemont, A. Bourassa, J. M. C. Plane, D. Klocke, S. A. Carn, L. Clarisse, T. Trickl, R. Neely, A. D. James, L. Rieger, J. C. Wilson and B. Meland, *Rev. Geophys.*, 2016, **54**, 278–335.
15 F. Arnold, R. Fabian and W. Joos, *Geophys. Res. Lett.*, 1981, **8**, 293–296.
16 A. A. Viggiano and F. Arnold, *Geophys. Res. Lett.*, 1981, **8**, 583–586.
17 S. Solomon, J. S. Daniel, R. R. Neely, J.-P. Vernier, E. G. Dutton and L. W. Thomason, *Science*, 2011, **333**, 866–870.
18 C. A. Brock, P. Hamill, J. C. Wilson, H. H. Jonsson and K. R. Chan, *Science*, 1995, **270**, 1650–1653.
19 R. G. Grainger and E. J. Highwood, Changes in stratospheric composition, chemistry, radiation and climate caused by volcanic eruptions, *Geological Society, London, Special Publications*, 2003, **213**, 329–347.
20 S. E. Bauer and D. Koch, *J. Geophys. Res.: Atmos.*, 2005, **110**, D17202.
21 D. K. Weisenstein, D. W. Keith and J. A. Dykema, *Atmos. Chem. Phys.*, 2015, **15**, 11835–11859.
22 R. W. Saunders, S. Dhomse, W. S. Tian, M. P. Chipperfield and J. M. C. Plane, *Atmos. Chem. Phys.*, 2012, **12**, 4387–4398.
23 T. Deshler, *J. Geophys. Res.*, 2003, **108**, 4167.
24 N. H. Farlow, V. R. Oberbeck, K. G. Snetsinger, G. V. Ferry, G. Polkowski and D. M. Hayes, *Science*, 1981, **211**, 832–834.
25 S. H. Jones, M. D. King and A. D. Ward, *Chem. Commun.*, 2015, **51**, 4914–4917.
26 L. Rkiouak, M. J. Tang, J. C. J. Camp, J. McGregor, I. M. Watson, R. A. Cox, M. Kalberer, A. D. Ward and F. D. Pope, *Phys. Chem. Chem. Phys.*, 2014, **16**, 11426–11434.
27 M. J. Tang, J. C. J. Camp, L. Rkiouak, J. McGregor, I. M. Watson, R. A. Cox, M. Kalberer, A. D. Ward and F. D. Pope, *J. Phys. Chem. A*, 2014, **118**, 8817–8827.
28 E. R. Garland, E. P. Rosen, L. I. Clarke and T. Baer, *Phys. Chem. Chem. Phys.*, 2008, **10**, 3156–3161.
29 Y. Li, M. J. Ezell and B. J. Finlayson-Pitts, *Atmos. Environ.*, 2011, **45**, 4123–4132.
30 A. K. Ray, B. Devakottai, A. Souyri and J. L. Huckaby, *Langmuir*, 1991, **7**, 525–531.
31 A. Abo Riziq, M. Trainic, C. Erlick, E. Segre and Y. Rudich, *Atmos. Chem. Phys.*, 2008, **8**, 1823–1833.
32 J. B. Gilman, T. L. Eliason, A. Fast and V. Vaida, *J. Colloid Interface Sci.*, 2004, **280**, 234–243.
33 E. González-Labrada, R. Schmidt and C. E. DeWolf, *Phys. Chem. Chem. Phys.*, 2007, **9**, 5814–5821.
34 M. D. King, A. R. Rennie, K. C. Thompson, F. N. Fisher, C. C. Dong, R. K. Thomas, C. Pfrang and A. V. Hughes, *Phys. Chem. Chem. Phys.*, 2009, **11**, 7699–7707.
35 C. Pfrang, F. Sebastiani, C. O. M. Lucas, M. D. King, I. D. Hoare, D. Chang and R. A. Campbell, *Phys. Chem. Chem. Phys.*, 2014, **16**, 13220–13228.
36 L. F. Voss, M. F. Bazerbashi, C. P. Beekman, C. M. Hadad and H. C. Allen, *J. Geophys. Res.: Atmos.*, 2007, **112**, D06209.
37 L. F. Voss, C. M. Hadad and H. C. Allen, *J. Phys. Chem. B*, 2006, **110**, 19487–19490.
38 M. D. King, S. H. Jones, C. O. M. Lucas, K. C. Thompson, A. R. Rennie, A. D. Ward, A. A. Marks, F. N. Fisher, C. Pfrang, A. V. Hughes and R. A. Campbell, *Phys. Chem. Chem. Phys.*, 2020, **22**, 28032–28044.
39 B. Woden, M. W. A. Skoda, A. Milsom, C. Gubb, A. Maestro, J. Tellam and C. Pfrang, *Atmos. Chem. Phys.*, 2021, **21**, 1325–1340.
40 F. Sebastiani, R. A. Campbell, K. Rastogi and C. Pfrang, *Atmos. Chem. Phys.*, 2018, **18**, 3249–3268.
41 S. H. Jones, M. D. King, A. D. Ward, A. R. Rennie, A. C. Jones and T. Arnold, *Atmos. Environ.*, 2017, **161**, 274–287.
42 R. H. Shepherd, M. D. King, A. A. Marks, N. Brough and A. D. Ward, *Atmos. Chem. Phys.*, 2018, **18**, 5235–5252.
43 M. N. Romanas, H. Ourrad, F. Thévenet and V. Riffault, *J. Phys. Chem. A*, 2016, **120**, 1197–1212.
44 M. J. Tang, P. J. Telford, F. D. Pope, L. Rkiouak, N. L. Abraham, A. T. Archibald, P. Braesicke, J. A. Pyle, J. McGregor, I. M. Watson, R. A. Cox and M. Kalberer, *Atmos. Chem. Phys.*, 2014, **14**, 6035–6048.
45 Y. Fang, M. Tang and V. H. Grassian, *J. Phys. Chem. A*, 2016, **120**, 4016–4024.
46 K. Gorkowski, H. Beydoun, M. Aboff, J. S. Walker, J. P. Reid and R. C. Sullivan, *Aerosol Sci. Technol.*, 2016, **50**, 1327–1341.
47 K. Gorkowski, N. M. Donahue and R. C. Sullivan, *Environ. Sci. Technol.*, 2017, **51**, 12154–12163.
48 K. Gorkowski, N. M. Donahue and R. C. Sullivan, *Environ. Sci.: Processes Impacts*, 2018, **20**, 1512–1523.
49 K. Gorkowski, N. M. Donahue and R. C. Sullivan, *Chem*, 2020, **6**, 204–220.
50 R. C. Sullivan, H. Boyer-Chelmo, K. Gorkowski and H. Beydoun, *Acc. Chem. Res.*, 2020, **53**, 2498–2509.
51 F. D. Pope, P. Braesicke, R. G. Grainger, M. Kalberer, I. M. Watson, P. J. Davidson and R. A. Cox, *Nat. Clim. Change*, 2012, **2**, 713–719.

52 K. E. McCusker, D. S. Battisti and C. M. Bitz, *Geophys. Res. Lett.*, 2015, **42**, 4989–4997.
53 A. Laakso, H. Kokkola, A.-I. Partanen, U. Niemeier, C. Timmreck, K. E. J. Lehtinen, H. Hakkarainen and H. Korhonen, *Atmos. Chem. Phys.*, 2016, **16**, 305–323.
54 D. Eatough, F. Caka and R. Farber, *Isr. J. Chem.*, 1994, **34**, 301–314.
55 P. J. Rasch, S. Tilmes, R. P. Turco, A. Robock, L. Oman, C.-C. J. Chen, G. L. Stenchikov and R. R. Garcia, *Philos. Trans. R. Soc., A*, 2008, **366**, 4007–4037.
56 A. D. Ward, M. Zhang and O. Hunt, *Opt. Express*, 2008, **16**, 16390–16403.
57 S. H. Jones, M. D. King and A. D. Ward, *Phys. Chem. Chem. Phys.*, 2013, **15**, 20735–20741.
58 G. David, K. Esat, I. Ritsch and R. Signorell, *Phys. Chem. Chem. Phys.*, 2016, **18**, 5477–5485.
59 Z. Gong, Y.-L. Pan, G. Videen and C. Wang, *J. Quantitat. Spectrosc. Radiat. Transfer*, 2018, **214**, 94–119.
60 F. A. Jenkins and H. White, *Fundamentals of optics*, McGraw-Hill, 2001.
61 U. K. Krieger, J. C. Mössinger, B. Luo, U. Weers and T. Peter, *Appl. Opt.*, 2000, **39**, 3691–3703.
62 E. Fällman and O. Axner, *Appl. Opt.*, 1997, **36**, 2107–2113.
63 C. Wang, Y.-L. Pan and G. Videen, *Meas. Sci. Technol.*, 2021, **32**, 102005.
64 C. F. Bohren and D. R. Huffman, *Absorption and Scattering of Light by Small Particles*, Wiley-VCH Verlag GmbH & Co, 2004.
65 A. K. Ray and R. Nandakumar, *Appl. Opt.*, 1995, **34**, 7759–7770.
66 A. L. Aden and M. Kerker, *J. Appl. Phys.*, 1951, **22**, 1242–1246.
67 O. B. Toon and T. P. Ackerman, *Appl. Opt.*, 1981, **20**, 3657–3660.
68 B. Vennes and T. C. Preston, *J. Opt. Soc. Am. A*, 2019, **36**, 2089.
69 B. Vennes and T. C. Preston, *Phys. Rev. A*, 2020, **101**, 063812.
70 E. E. Remsberg, D. Lavery and B. Crawford, *J. Chem. Eng. Data*, 1974, **19**, 263–265.
71 K. F. Palmer and D. Williams, *Appl. Opt.*, 1975, **14**, 208–219.
72 R. T. Tisdale, D. L. Glandorf, M. A. Tolbert and O. B. Toon, *J. Geophys. Res.: Atmos.*, 1998, **103**, 25353–25370.
73 R. F. Niedziela, M. L. Norman, R. E. Miller and D. R. Worsnop, *Geophys. Res. Lett.*, 1998, **25**, 4477–4480.
74 H. M. Steele and P. Hamill, *J. Aerosol Sci.*, 1981, **12**, 517–528.
75 R. Wagner, S. Benz, H. Bunz, O. Möhler, H. Saathoff, M. Schnaiter, T. Leisner and V. Ebert, *J. Phys. Chem. A*, 2008, **112**, 11661–11676.
76 C. E. Lund Myhre, D. H. Christensen, F. M. Nicolaisen and C. J. Nielsen, *J. Phys. Chem. A*, 2003, **107**, 1979–1991.
77 R. Wagner, S. Benz, H. Bunz, O. Möhler, H. Saathoff, M. Schnaiter, T. Leisner and V. Ebert, *J. Phys. Chem. A*, 2008, **112**, 11661–11676.
78 O. R. Hunt, A. D. Ward and M. D. King, *RSC Adv.*, 2013, **3**, 19448.
79 I. H. Malitson, *J. Opt. Soc. Am.*, 1965, **55**, 1205–1209.
80 C. Mund and R. Zellner, *ChemPhysChem*, 2003, **4**, 638–645.
81 *Handbook of Chemistry and Physics*, 97th edn, ed. W. M. Haynes, CRC Press, 2016.
82 Z. Hu and D. C. Ripple, *J. Res. Natl. Inst. Stand. Technol.*, 2014, **119**, 674–682.
83 J. P. Reid, B. J. Dennis-Smither, N.-O. A. Kwamena, R. E. H. Miles, K. L. Hanford and C. J. Homer, *Phys. Chem. Chem. Phys.*, 2011, **13**, 15559.
84 Y. Qiu and V. Molinero, *J. Am. Chem. Soc.*, 2015, **137**, 10642–10651.
85 R. E. O'Brien, B. Wang, S. T. Kelly, N. Lundt, Y. You, A. K. Bertram, S. R. Leone, A. Laskin and M. K. Gilles, *Environ. Sci. Technol.*, 2015, **49**, 4995–5002.
86 C. Cai, R. E. H. Miles, M. I. Cotterell, A. Marsh, G. Rovelli, A. M. J. Rickards, Y.-H. Zhang and J. P. Reid, *J. Phys. Chem. A*, 2016, **120**, 6604–6617.
87 Y. You and A. K. Bertram, *Atmos. Chem. Phys.*, 2015, **15**, 1351–1365.
88 Y. Wu, T. Cheng, X. Gu, L. Zheng, H. Chen and H. Xu, *J. Quantitat. Spectrosc. Radiat. Transfer*, 2014, **135**, 9–19.
89 A. Soewono and S. N. Rogak, *Aerosol Sci. Technol.*, 2013, **47**, 267–274.
90 M. Kahnert, T. Nousiainen and H. Lindqvist, *Opt. Express*, 2013, **21**, 7974–7993.
91 Y. Wu, T. Cheng, L. Zheng and H. Chen, *J. Quantitat. Spectrosc. Radiat. Transfer*, 2016, **182**, 1–11.
92 S. China, C. Mazzoleni, K. Gorkowski, A. C. Aiken and M. K. Dubey, *Nat. Commun.*, 2013, **4**, 2122.
93 T. Koop, B. Luo, A. Tsias and T. Peter, *Nature*, 2000, **406**, 611–614.
94 T. Koop, *Z. Phys. Chem.*, 2004, **218**, 1231–1258.
95 T. Koop, Atmospheric Water, in *Water: Fundemental as the bassi for undestanding the environment and promoting technology*, ed. P. G. Debenedetti, A. Ricci and F. Bruni, IOS Press, Amsterdam, Bologna, 2015, pp. 45–75.
96 J. Schneider, K. Höhler, R. Wagner, H. Saathoff, M. Schnaiter, T. Schorr, I. Steinke, S. Benz, M. Baumgartner, C. Rolf, M. Krämer, T. Leisner and O. Möhler, *Atmos. Chem. Phys.*, 2021, **21**, 14403–14425.
97 T. Ohtake, *Tellus B*, 1993, **45**, 138–144.
98 N. Song, *Geophys. Res. Lett.*, 1994, **21**, 2709–2712.
99 A. K. Bertram, D. D. Patterson and J. J. Sloan, *J. Phys. Chem.*, 1996, **100**, 2376–2383.
100 M. L. Clapp, R. F. Niedziela, L. J. Richwine, T. Dransfield, R. E. Miller and D. R. Worsnop, *J. Geophys. Res.: Atmos.*, 1997, **102**, 8899–8907.
101 Y. Chen, P. J. DeMott, S. M. Kreidenweis, D. C. Rogers and D. E. Sherman, *J. Atmos. Sci.*, 2000, **57**, 3752–3766.
102 H. Vortisch, B. Krämer, I. M. Weidinger, L. Wöste, T. Leisner, M. Schwell, H. Baumgärtel and E. Rühl, *Phys. Chem. Chem. Phys.*, 2000, **2**, 1407–1413.
103 A. J. Prenni, M. E. Wise, S. D. Brooks and M. A. Tolbert, *J. Geophys. Res.: Atmos.*, 2001, **106**, 3037–3044.
104 D. J. Cziczo and J. P. D. Abbatt, *Geophys. Res. Lett.*, 2001, **28**, 963–966.
105 O. Möhler, O. Stetzer, S. Schaefers, C. Linke, M. Schnaiter, R. Tiede, H. Saathoff, M. Krämer, A. Mangold, P. Budz,

P. Zink, J. Schreiner, K. Mauersberger, W. Haag, B. Kärcher and U. Schurath, *Atmos. Chem. Phys.*, 2003, **3**, 211–223.
106 M. Ettner, S. K. Mitra and S. Borrmann, *Atmos. Chem. Phys.*, 2004, **4**, 1925–1932.
107 A. Mangold, R. Wagner, H. Saathoff, U. Schurath, C. Giesemann, V. Ebert, M. Krämer and O. Möhler, *Meteorol. Z.*, 2005, **14**, 485–497.
108 M. R. Beaver, M. J. Elrod, R. M. Garland and M. A. Tolbert, *Atmos. Chem. Phys.*, 2006, **6**, 3231–3242.
109 Z. A. Kanji and J. P. D. Abbatt, *Aerosol Sci. Technol.*, 2009, **43**, 730–738.
110 B. D. Swanson, *J. Atmos. Sci.*, 2009, **66**, 741–754.
111 J. H. Seinfeld and S. N. Pandis, *Atmospheric Chemistry and Physics*, John Wiley and Sons, Inc., 1997.

